



**HAL**  
open science

## Mechanistic Insights into the Retaining Glucosyl-3-phosphoglycerate Synthase from Mycobacteria\*

Saioa Urresti, David Albesa-Jové, Francis Schaeffer, Ha T. Pham, Devinder Kaur, Petra Gest, Mark J. van Der Woerd, Ana Carreras-González, Sonia López-Fernández, Pedro M. Alzari, et al.

► **To cite this version:**

Saioa Urresti, David Albesa-Jové, Francis Schaeffer, Ha T. Pham, Devinder Kaur, et al.. Mechanistic Insights into the Retaining Glucosyl-3-phosphoglycerate Synthase from Mycobacteria\*. *Journal of Biological Chemistry*, 2012, 287 (29), pp.24649-24661. 10.1074/jbc.M112.368191 . pasteur-03137922

**HAL Id: pasteur-03137922**

**<https://pasteur.hal.science/pasteur-03137922>**

Submitted on 10 Feb 2021

**HAL** is a multi-disciplinary open access archive for the deposit and dissemination of scientific research documents, whether they are published or not. The documents may come from teaching and research institutions in France or abroad, or from public or private research centers.

L'archive ouverte pluridisciplinaire **HAL**, est destinée au dépôt et à la diffusion de documents scientifiques de niveau recherche, publiés ou non, émanant des établissements d'enseignement et de recherche français ou étrangers, des laboratoires publics ou privés.



Distributed under a Creative Commons Attribution 4.0 International License

# Mechanistic Insights into the Retaining Glucosyl-3-phosphoglycerate Synthase from Mycobacteria<sup>\*S</sup>

Received for publication, April 25, 2012, and in revised form, May 23, 2012. Published, JBC Papers in Press, May 25, 2012, DOI 10.1074/jbc.M112.368191

Saïoa Urresti<sup>†S1</sup>, David Albesa-Jové<sup>†S1</sup>, Francis Schaeffer<sup>¶1</sup>, Ha T. Pham<sup>||</sup>, Devinder Kaur<sup>||</sup>, Petra Gest<sup>||</sup>, Mark J. van der Woerd<sup>\*\*</sup>, Ana Carreras-González<sup>‡S</sup>, Sonia López-Fernández<sup>‡S</sup>, Pedro M. Alzari<sup>¶</sup>, Patrick J. Brennan<sup>||</sup>, Mary Jackson<sup>||2</sup>, and Marcelo E. Guerin<sup>‡S#†3</sup>

From the <sup>†</sup>Unidad de Biofísica, Centro Mixto Consejo Superior de Investigaciones Científicas-Universidad del País Vasco/Euskal Herriko Unibertsitatea, Barrio Sarriena s/n, Leioa, Bizkaia, 48940, Spain, the <sup>S</sup>Departamento de Bioquímica, Universidad del País Vasco, Spain, the <sup>¶</sup>Unité de Microbiologie Structurale and CNRS URA 2185, Institut Pasteur, 25 Rue du Dr. Roux, 75724 Paris Cedex 15, France, the <sup>||</sup>Mycobacteria Research Laboratories, Departments of Microbiology, Immunology, and Pathology and <sup>\*\*</sup>Biochemistry and Molecular Biology, Colorado State University, Fort Collins, Colorado 80523-1682, and the <sup>‡</sup>IKERBASQUE, Basque Foundation for Science, 48011, Bilbao, Spain

**Background:** Knowledge of conformational changes occurring in glycosyltransferases is limited.

**Results:** The active site of GpgS is essentially preformed as the protein proceeds along the catalytic cycle with the nucleotide sugar  $\beta$ -phosphate playing a central role in substrate binding.

**Conclusion:** Conformational dynamics is a major determinant of GpgS activity.

**Significance:** This model of action might be operational in other GT-A glycosyltransferases.

Considerable progress has been made in recent years in our understanding of the structural basis of glycosyl transfer. Yet the nature and relevance of the conformational changes associated with substrate recognition and catalysis remain poorly understood. We have focused on the glucosyl-3-phosphoglycerate synthase (GpgS), a “retaining” enzyme, that initiates the biosynthetic pathway of methylglucose lipopolysaccharides in mycobacteria. Evidence is provided that GpgS displays an unusually broad metal ion specificity for a GT-A enzyme, with  $Mg^{2+}$ ,  $Mn^{2+}$ ,  $Ca^{2+}$ ,  $Co^{2+}$ , and  $Fe^{2+}$  assisting catalysis. In the crystal structure of the apo-form of GpgS, we have observed that a flexible loop adopts a double conformation  $L_A$  and  $L_I$  in the active site of both monomers of the protein dimer. Notably, the  $L_A$  loop geometry corresponds to an active conformation and is conserved in two other relevant states of the enzyme, namely the GpgS·metal·nucleotide sugar donor and the GpgS·metal·nucleotide·acceptor-bound complexes, indicating that GpgS is intrinsically in a catalytically active conformation. The crystal structure of GpgS in the presence of  $Mn^{2+}$ ·UDP-phosphoglyceric acid revealed an alternate conforma-

tion for the nucleotide sugar  $\beta$ -phosphate, which likely occurs upon sugar transfer. Structural, biochemical, and biophysical data point to a crucial role of the  $\beta$ -phosphate in donor and acceptor substrate binding and catalysis. Altogether, our experimental data suggest a model wherein the catalytic site is essentially preformed, with a few conformational changes of lateral chain residues as the protein proceeds along the catalytic cycle. This model of action may be applicable to a broad range of GT-A glycosyltransferases.

Glycosyltransferases (GTs)<sup>4</sup> play a central role in nature due to their exceptional capacity to synthesize a broad range of glycans. They transfer a sugar moiety from nucleotide sugar and lipid-phosphosugar donors to acceptor substrates, including mono-, oligo-, and polysaccharides, proteins, lipids, small organic molecules, and deoxyribonucleic acids (1). GTs can be classified as either “retaining” or “inverting” enzymes according to the anomeric configuration of substrates and products (2). Inverting GTs follow a direct displacement  $S_N2$ -like mechanism via a single oxocarbenium ion-like state. In contrast, the catalytic mechanism for retaining GTs remains less clear. By analogy with glycosylhydrolases, a double displacement mechanism involving a covalently bound glycosyl-enzyme intermediate was first suggested. However, in the absence of both, a clear catalytic nucleophile and structural/kinetic evidence of a viable covalent intermediate, an alternative mechanism has been proposed. In this mechanism, known as “internal return,” leaving group departure and nucleophilic attack occur on the same face of the sugar (3–7) involving either a short lived oxocarbenium ion intermediate ( $SNi$ -like) (8) or an oxocarbenium

\* This work was supported, in whole or in part, by National Institutes of Health Grant AI064798 from NIAID. This work was also supported by European Commission Contract LSHP-CT-2005-018923 (New Medicines for Tuberculosis), More Medicines for Tuberculosis Contract HEALTH-F3-2011-260872, the Spanish Ministry of Science and Innovation Contract SAF2010-19096, IKERBASQUE, the Basque Foundation for Science, and the Fundación Biofísica Bizkaia.

<sup>S</sup> This article contains supplemental Experimental Procedures and Fig. S1. The atomic coordinates and structure factors (codes 4DDZ, 4DE7, and 4DEC) have been deposited in the Protein Data Bank, Research Collaboratory for Structural Bioinformatics, Rutgers University, New Brunswick, NJ (<http://www.rcsb.org/>).

<sup>1</sup> These authors contributed equally to this work.

<sup>2</sup> To whom correspondence may be addressed. Tel.: 970-491-3582; Fax: 970-491-1815; E-mail: Mary.Jackson@colostate.edu.

<sup>3</sup> To whom correspondence may be addressed: Unidad de Biofísica, Centro Mixto Consejo Superior de Investigaciones Científicas-Universidad del País Vasco/Euskal Herriko Unibertsitatea, Barrio Sarriena s/n, Leioa, Bizkaia, 48940, Spain. Tel.: 34-94-601-8052; Fax: 34-94-601-3360; E-mail: mrcguerin@gmail.com.

<sup>4</sup> The abbreviations used are: GT, glycosyltransferase; AUC, analytical ultracentrifugation; ITC, isothermal titration calorimetry; PGA, 3-phosphoglycerate; URI, uridine; MGLP, 6-O-methylglucose lipopolysaccharide; r.m.s.d., root mean square deviation; GpgS, glucosyl-3-phosphoglycerate synthase.

ion transition state (S<sub>N</sub>i) (9). Two major structural folds have been described for the nucleotide sugar-dependent enzymes among the first 35 GT sequence-based families (CAZy, carbohydrate-active enzymes database (10)) for which three-dimensional structures have been reported. These topologies are variations of “Rossmann-like” domains and have been identified as GT-A and GT-B (11, 12). Moreover, bioinformatics analysis revealed that many of the structurally uncharacterized nucleotide sugar-dependent GT families are also predicted to adopt one of these two folds. Interestingly, both inverting and retaining enzymes were found in GT-A and GT-B folds indicating that there is no correlation between the overall fold of GTs and their catalytic mechanism. The GT-A fold was first described for the 256-amino acid protein SpsA from family GT2, a putative inverting GT from *Bacillus subtilis* (13). It consists of two tightly associated  $\beta/\alpha/\beta$  Rossmann-like domains, where the N-terminal domain recognizes the nucleotide sugar donor and the C-terminal domain of the protein contains the acceptor-binding site. Most GT-A enzymes exhibit an Asp-Xaa-Asp (also known as DXD) signature in which the carboxylate groups coordinate a divalent cation and/or a ribose ring (2). Kinetic and structural studies have revealed that most GT-A enzymes follow an ordered mechanism in which the divalent cation and nucleotide sugar donor bind first, prior to binding of the acceptor (14–16). The glycosylated acceptor is then released, followed by the nucleotide group. The divalent cation may react with the free enzyme and does not dissociate after each catalytic cycle (17–23). Often the interaction of GT enzymes with their natural substrates leads to substantial changes in the structural conformation of the proteins, compared with their free forms, with direct implications for their function (12, 24, 25). Specific loops, adjacent to the active site, for instance, often adopt different conformations in the presence or absence of substrates. These loops have been suggested to restrict water access to the active site and appear to play a crucial role during substrate binding and catalysis in GT-A enzymes, including inverting G<sub>N</sub>T-I (26),  $\beta$ 4Gal-T1 (21), GlcAT-I (27), CstII (28), and MgS (29) and retaining  $\alpha$ -(1,3)GalT (20, 30) and GTA/GTB (31).

The glucosyl-3-phosphoglycerate synthase (GpgS) is a retaining  $\alpha$ -glucosyltransferase that initiates the biosynthetic pathway of the 6-O-methylglucose lipopolysaccharides (MGLPs) in mycobacteria. The enzyme transfers a Glc<sub>p</sub> moiety from UDP-Glc to the 2-position of the 3-phosphoglycerate (PGA) to form glucosyl 3-phosphoglycerate (Fig. 1A) (31, 33). MGLPs are cytoplasmic lipopolysaccharides of intermediate size containing up to 20 Glc<sub>p</sub> units, many of which are 6-O-methylated. Moreover, MGLPs can be acylated with additional acetyl, propionyl, isobutyryl, succinyl, and octanoyl groups (Fig. 1B) (34). A remarkable property associated with MGLPs is their ability to form stable 1:1 complexes with long-chain fatty acids and acyl-coenzyme A derivatives *in vitro* (35, 36). The fact that MGLPs are composed of Glc<sub>p</sub> units predominantly in  $\alpha$ -(1→4)-linkage confers on these molecules a proclivity to assume an helical conformation. Within the complexes, the fatty acyl chain is included in the nonpolar cavity of the coiled polysaccharide chain (37). Interestingly, with an intracellular concentration of long-chain acyl-CoAs in *Mycobacterium smegmatis* of ~0.3 mM, the concentration of polymethylated polysaccharides

approaching 1 mM, and the dissociation constant of the polysaccharide·lipid complex estimated to 0.1  $\mu$ M, all of the long-chain fatty acids of the cytosol may form complexes with polymethylated polysaccharides leading to the suggestion that the physiological function of these polymethylated polysaccharides may serve to as general carriers for long-chain fatty acids synthesized in the cytosol (38).

This study describes a detailed investigation of the conformational properties of MtGpgS in solution. Using a combination of x-ray crystallography, limited proteolysis, isothermal titration calorimetry (ITC), and analytical ultracentrifugation (AUC), we propose a plausible model for donor and acceptor substrate recognition and binding. The implications of this model for the understanding of the early steps of MGLPs biosynthesis and the catalytic mechanism of other members of the GT-A family are discussed.

### EXPERIMENTAL PROCEDURES

**Methods**—Recombinant glucosyl-3-phosphoglycerate synthase from *Mycobacterium tuberculosis* (MtGpgS, Rv1208) was produced in *Escherichia coli* and purified to apparent homogeneity as described (39).

**GpgS Enzymatic Activity Measurements**—GpgS activity was measured as described previously with minor modifications (33). The reaction mixture contained 3  $\mu$ g of recombinant purified MtGpgS, 0.5 mM (0.05  $\mu$ Ci) UDP-D-[U-<sup>14</sup>C]Glc (GE Healthcare), 1–3 mM D-3-phosphoglyceric acid (Sigma), 20 mM divalent cation salt (MgCl<sub>2</sub>, MnCl<sub>2</sub>, FeCl<sub>2</sub>, CuCl<sub>2</sub>, CaCl<sub>2</sub>, ZnCl<sub>2</sub>, and CoCl<sub>2</sub>), and 25 mM Tris-HCl buffer, pH 8.0, in a total volume of 100  $\mu$ l. All buffers were treated with Chelex 100 resin prior to the addition of the various salts to ensure the removal of any residual traces of divalent cations. Reaction mixtures were incubated at 37 °C for 20 min. Reaction products were separated by TLC on aluminum-backed silica gel 60-precoated plates F254 developed in 1-propanol/ethyl acetate/water/25% ammonia (50:10:30:10) and semi-quantified by using a PhosphorImager Typhoon TRIO (GE Healthcare).

**GpgS Crystallization and Data Collection**—The apo-forms of MtGpgS and MtGpgS in complex with Mg<sup>2+</sup> and uridine 5'-diphosphate (UDP, Fluka; MtGpgS·Mg<sup>2+</sup>·UDP) were crystallized as described previously (39). Crystals of MtGpgS in complex with Mn<sup>2+</sup>, UDP, and PGA (MtGpgS·Mn<sup>2+</sup>·UDP·PGA) were obtained by mixing 0.5  $\mu$ l of the protein (10 mg ml<sup>-1</sup>) in the presence of 5 mM MnCl<sub>2</sub>, 5 mM UDP, and 5 mM PGA with 0.5  $\mu$ l of a mother liquor of 0.4 M NH<sub>4</sub> dihydrogen phosphate using the sitting drop vapor diffusion method. Crystals appeared after 1–2 days and grew as rhombuses reaching 0.37 × 0.30 × 0.15 mm. Prior to data collection, the crystals were cryo-cooled in liquid nitrogen by using 0.5 M NH<sub>4</sub> dihydrogen phosphate and 30% (v/v) glycerol as cryo-protectant solution. X-ray diffraction data from single crystals of MtGpgS·Mn<sup>2+</sup>·UDP·PGA were collected using synchrotron radiation in the ID-23-2 microfocus beamline ( $\lambda$  = 0.873 Å) at the European Synchrotron Radiation Facility (ESRF, Grenoble, France), and processed with the XDS program. MtGpgS·Mn<sup>2+</sup>·UDP·PGA crystals belong to the I<sub>4</sub> space group and diffracted to 1.98 Å and have two monomers per asymmetric unit, corresponding to a Matthews coefficient of 2.32 Å<sup>3</sup> and a

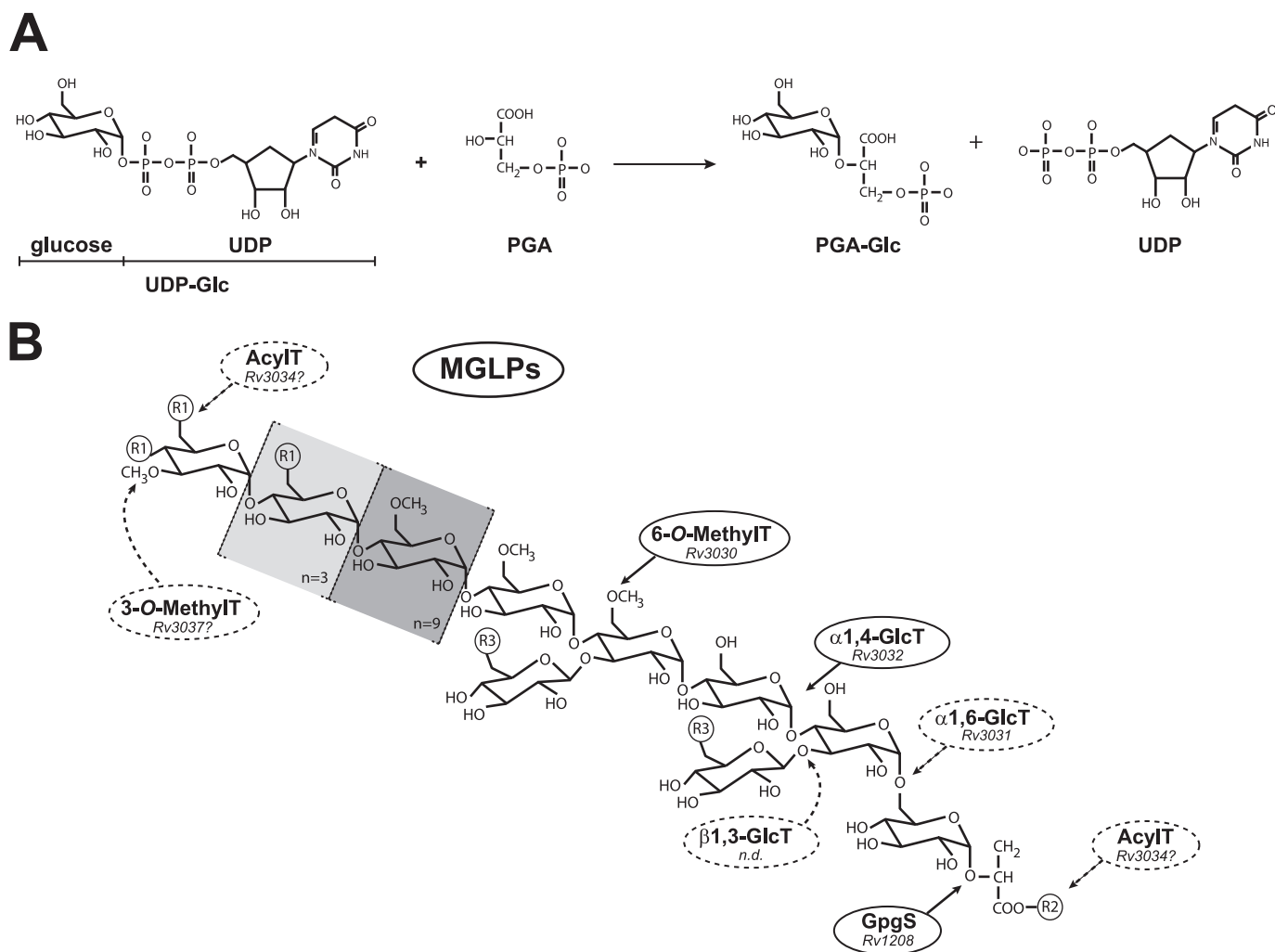


FIGURE 1. **MGLP biosynthesis in mycobacteria.** *A*, glucosyl-3-phosphoglycerate biosynthesis in mycobacteria. GpgS transfers a GlcP residue from UDP-GlcP to the 2-position of 3-phosphoglycerate to form glucosyl-3-phosphoglycerate. The reaction occurs with retention of the anomeric configuration of the sugar donor. *B*, MGLPs chemical structure. The MGLPs from *Mycobacterium bovis* BCG are composed of 10  $\alpha$ -(1 $\rightarrow$ 4)-linked 6-O-methylglucosyl residues with a nonreducing end made of the tetrasaccharide 3-O-methyl-D-GlcP-( $\alpha$ -(1 $\rightarrow$ 4)-D-GlcP)<sub>3</sub>- $\alpha$ -(1 $\rightarrow$ ). The tetrasaccharide  $\rightarrow$ 4)-( $\alpha$ -(1 $\rightarrow$ 4)-D-GlcP)<sub>3</sub>- $\alpha$ -(1 $\rightarrow$ 6)-D-GlcP- $\alpha$ -(1 $\rightarrow$ ) linked to position 2 of D-glyceric acid constitutes the reducing end of the molecule) (66). Position 3 of the second and that of fourth  $\alpha$ -D-GlcP residues (closest to the reducing end) are substituted by single  $\alpha$ -D-GlcP residues. R1, R2, and R3 are acyl groups: R1, acetate, propionate, or isobutyrate; R2, octanoate; and R3, succinate. MGLPs occur as a mixture of four main components that differ in their content of esterified succinate. The names of the genes thought to be involved in the different steps of their elongation and modifications are shown (32, 67). Acylation and methylation are thought to occur concurrently; the precise stage at which the two  $\beta$ -(1 $\rightarrow$ 3)-linked Glc residues are attached is not known, but the definition of early MGLP precursors suggests that they are added early during the elongation process.

solvent content of 47.04%. The complete data collection statistics are shown in Table 1.

**Structure Determination and Refinement**—The structures of the apo-form of MtGpgS and that of the MtGpgS·Mg<sup>2+</sup>·UDP and MtGpgS·Mn<sup>2+</sup>·UDP·PGA complexes were solved by molecular replacement with the program Phaser Version 2.1.2 (40), using the atomic coordinates of MAP2569c from *Mycobacterium avium* subsp. *paratuberculosis* as the search model (Protein Data Bank code 1CKJ, see Ref. 41). The final MtGpgS apo-form, MtGpgS·Mg<sup>2+</sup>·UDP, and MtGpgS·Mn<sup>2+</sup>·UDP·PGA models were obtained after alternate cycles of model building using the program COOT (42) and restrained refinement using the program phenix.refine (43).

**Limited Proteolysis of MtGpgS**—Recombinant purified MtGpgS (25  $\mu$ g) was incubated with 10 mM MnCl<sub>2</sub> and 0.10  $\mu$ g of trypsin (Sigma) in 100  $\mu$ l of 20 mM Tris-HCl, pH 7.5, in the

presence of 1 mM uridine (URI, Sigma), 1 mM uridine 5'-monophosphate (UMP, Sigma), 1 mM UDP, 1 mM uridine 5'-diphosphate glucose (UDP-Glc, Sigma), and/or 1.25 mM PGA for 0–90 min at 37 °C. Aliquots of 12  $\mu$ l were mixed with 3  $\mu$ l of 250 mM Tris-HCl, pH 6.8, 10% SDS, 50% glycerol, 500 mM DTT, and 0.01% bromphenol blue at the indicated times. Samples were boiled for 3 min and run in a NuPAGE<sup>®</sup> 4–12% gel (Invitrogen). Protein bands were visualized by staining with SimplyBlue<sup>™</sup> SafeStain (Invitrogen).

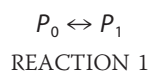
**N-terminal Sequence Analyses**—Samples were run in a NuPAGE<sup>®</sup> 4–12% gel. The gel was then washed with NuPAGE<sup>®</sup> transfer buffer (Invitrogen) during 15 min at room temperature. Proteolytic fragments were electrotransferred to a PVDF membrane using the iBlot dry blotting system (Invitrogen) during 7 min. The PVDF membrane was then washed for 10 min with Milli-Q<sup>®</sup> purified water. Bands were stained with a

## Conformational Dynamics in GT-A Glycosyltransferases

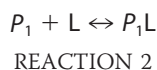
solution containing 0.1% Coomassie Brilliant Blue R-250, 40% methanol, and 1% acetic acid and subjected to N-terminal sequence analysis using Applied Biosystems 494 precise high throughput protein sequencer at the Biomolecular Resource Facility of the University of Texas Medical Branch.

**Isothermal Titration Calorimetry**—Ligand binding to *MtGpgS* was assayed using the VP-ITC system (MicroCal Inc.) as described previously (25, 44), with the following modifications. The ITC cell (1.4 ml) contained 40  $\mu\text{M}$  *MtGpgS* in 50 mM HEPES, pH 7.5, 2 mM  $\text{MnCl}_2$ , 150 mM NaCl, and the syringe (300  $\mu\text{l}$ ) contained 500  $\mu\text{M}$  of URI, UMP, UDP, UDP-Glc, or PGA in the same buffer. Binding of PGA to *MtGpgS*-UDP and uridine complexes was assayed as follows. *MtGpgS* was first titrated with the nucleotide analogs, and the resulting solutions of the protein nucleotide complexes were then titrated with a 500  $\mu\text{M}$  PGA solution. Sample solutions were thoroughly degassed under vacuum, and each titration was performed at the indicated temperature by one injection of 2  $\mu\text{l}$  followed by 37 injections of 8  $\mu\text{l}$ , with 210 s between injections using a 416 rpm rotating syringe. Raw heat signal collected with a 16-s filter was corrected for the dilution heat of the ligand in the *MtGpgS* buffer and normalized to the concentration of ligand injected. UMP, uridine, and PGA binding isotherms were fitted to a single site bi-molecular model (45) using the Origin<sup>TM</sup> software provided by the manufacturer. Fitting the UDP-Glc and UDP binding isotherms required to develop a specific binding algorithm as described below.

**Analysis of UDP and UDP-Glc Binding Isotherms**—ITC binding isotherms observed upon UDP and UDP-Glc binding to GpgS were fitted to a model considering two equilibrium reactions, the equilibrium between two protein conformations,  $P_0$  and a  $P_1$  (Reaction 1),



with equilibrium constant  $K_e$  and thermodynamic parameters  $\Delta G_e$ ,  $\Delta H_e$ ,  $\Delta S_e$ , and  $\Delta C_{p,e}$ , and the binding equilibrium with 1:1 stoichiometry between one free protein conformation only,  $P_1$ , and its bound complex (Reaction 2),



with equilibrium constant  $K_b$  and thermodynamic parameters  $\Delta G_b$ ,  $\Delta H_b$ ,  $\Delta S_b$ , and  $\Delta C_{p,b}$ . The GpgS protein population shifts upon ligand binding from free  $P_0$  to bound  $P_1$  conformations with the overall equilibrium constant  $K = K_e \cdot K_b$ . The heat absorbed or evolved upon ligand addition to the GpgS solution is the sum of the heats absorbed or evolved during equilibration of the two protein equilibria,  $dQ = dQ_e + dQ_b$ . The experimental parameter determined in the titration calorimeter is the differential heat  $dQ/dL_{\text{tot}}$  (actually  $\Delta Q/\Delta L_{\text{tot}}$ ), where  $L_{\text{tot}}$  is the total ligand concentration, free plus bound (see Equations 1–3 and supplemental material)

$$\frac{dQ}{dL_{\text{tot}}} = \frac{dQ_e}{dL_{\text{tot}}} + \frac{dQ_b}{dL_{\text{tot}}} \quad (\text{Eq. 1})$$

$$\frac{dQ_e}{dL_{\text{tot}}} = -\frac{\Delta H_e V_0}{2\alpha} \left( 1 + \frac{r + (L_r - 1)/\alpha}{((r + (L_r - 1)/\alpha)^2 + 4r/\alpha)^{1/2}} \right) \quad (\text{Eq. 2})$$

$$\frac{dQ_b}{dL_{\text{tot}}} = \frac{\Delta H_b V_0}{2} \left( 1 - \frac{L_r + \alpha r - 1}{((L_r + \alpha r + 1)^2 - 4L_r)^{1/2}} \right) \quad (\text{Eq. 3})$$

$L_r$  and  $r$  are two unitless parameters that depend on the total ligand and protein concentrations,  $r = 1/P_{\text{tot}} K_b$ ,  $L_r = L_{\text{tot}}/P_{\text{tot}}$  (45), and  $\alpha$  is a unitless parameter that depends on the equilibrium constant between the two protein conformations,  $\alpha = 1 + 1/K_e$ .  $V_0$  is the reaction cell volume. Nonlinear regression analysis of  $dQ/dL_{\text{tot}}$  (Equation 1) allows estimation of the thermodynamic parameters of the two equilibrium reactions.

**Analytical Ultracentrifugation**—AUC experiments were performed with a Beckman XL-1 analytical ultracentrifuge using absorbance optics. Velocity measurements utilized two-sector charcoal-filled Epon centerpieces, quartz windows, 400- $\mu\text{l}$  sample and 420- $\mu\text{l}$  reference volumes in 50 mM Tris-HCl, pH 8.0, 150 mM NaCl. All samples were centrifuged in a Beckman 8-hole An50Ti rotor at 22  $^\circ\text{C}$  at 40,000 rpm, and the data were collected at 280 nm, with a radial increment of 0.003 cm for  $\sim 7$  h. Velocity data were edited and analyzed using the boundary analysis method of Demeler and van Holde as implemented in Ultrascan version 7.3 for Windows (46). Sedimentation coefficients ( $s$ ) are reported in Svedberg units (S), where 1 S =  $1 \times 10^{-13}$  s and were corrected to that of water at 20  $^\circ\text{C}$  ( $s_{20,w}$ ). The partial specific volume of full-length *MtGpgS* was calculated from the amino acid sequence within Ultrascan. Modeling of hydrodynamic parameters was performed using Ultrascan. The frictional ratio ( $f/f_0$ ) was calculated from the known molecular mass and measured sedimentation coefficient using Ultrascan.

**Structural Alignment**—Structural alignment of *MtGpgS* (Protein Data Bank codes 4DDZ, 4DE7, and 4DEC are from this study; 3E25 and 3E26 are from Ref. 47), *MaGpgS* (3CKJ), 3CKN, 3CKO, 3CKQ, and 3CKV are from Ref. 41), and other GT-A glycosyltransferases was performed by the distance alignment matrix method using DALI Lite. Molecular graphics and analyses were performed with the UCSF Chimera package (48).

## RESULTS AND DISCUSSION

**Metal Ion Promiscuity in *MtGpgS***—In most GT-A glycosyltransferases, metal ions play a central role in substrate recognition and catalysis (2, 23). Specifically, in *MtGpgS*, the conserved His<sup>258</sup> residue and the carboxylate groups of the Asp<sup>134</sup>–Ser<sup>135</sup>–Asp<sup>136</sup> signature are involved in divalent metal cation coordination, which also coordinates to the  $\alpha$ - and  $\beta$ -phosphate moieties of the donor substrate UDP-Glc. The divalent metal cation has been proposed to play the role of the Lewis acid during catalysis in retaining GT-A enzymes and is an essential co-factor for enzymatic activity in *MtGpgS* (Fig. 2) (2). Therefore, we decided to investigate the influence of several metal ions on the activity of the enzyme. In contrast to previous reports (49, 50), we found that *MtGpgS* was not only active in the presence of  $\text{Mg}^{2+}$  but also when other metal cations were used as co-factors. As depicted in Fig. 2, the enzyme requires

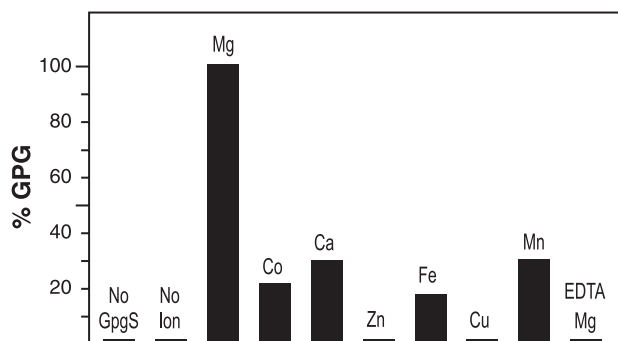


**FIGURE 2. Role of metal ions in *MtGpgS* enzymatic activity.** The *MtGpgS* activity was measured by incubating the recombinant enzyme in the presence of UDP-D-[U-<sup>14</sup>C]Glc, D-3-phosphoglyceric acid (Sigma), and a broad range of metal ion salts as follows: 1st lane, no enzyme added; 2nd lane, no metal ion added; 3rd lane, MgCl<sub>2</sub>; 4th lane, CoCl<sub>2</sub>; 5th lane, CaCl<sub>2</sub>; 6th lane, ZnCl<sub>2</sub>; 7th lane, FeCl<sub>2</sub>; 8th lane, CuCl<sub>2</sub>; 9th lane, MnCl<sub>2</sub>; 10th lane, MgCl<sub>2</sub> and EDTA (for details see "Experimental Procedures").

Mg<sup>2+</sup> for maximal activity. However, *MtGpgS* was enzymatically active when another group II metal ion (Ca<sup>2+</sup>) and transition metal ions (Mn<sup>2+</sup>, Co<sup>2+</sup>, or Fe<sup>2+</sup>) were present in the reaction mixture. *MtGpgS* was not active in the presence of Zn<sup>2+</sup> or Cu<sup>2+</sup>. Our results thus point to a relatively broad specificity of GpgS for metal cations.

**Dynamic Loop as Key Factor in *MtGpgS*-mediated Catalysis**—The first described crystal structure of a mycobacterial GpgS (GT81 family) was that of *M. avium* subsp. *paratuberculosis* (*MaGpgS*; apo-form and Mn<sup>2+</sup>·UDP, Mn<sup>2+</sup>·UDP-Glc, UDP-Glc and UDP-GlcNAc complexed forms; Ref. 41) followed by that of *M. tuberculosis* (*MtGpgS*; apo-form and Mg<sup>2+</sup>·UDP-PGA complexed form (47), and apo-form, Mg<sup>2+</sup>·UDP and Mn<sup>2+</sup>·UDP-PGA (Table 1)). *MaGpgS* and *MtGpgS* are structurally closely related enzymes (root mean square deviation value of 1.4 Å) displaying an 82% sequence identity and 95% sequence similarity. Both *MaGpgS* and *MtGpgS* are homodimers and display the characteristic two tightly bound domain organization of GT-A glycosyltransferases (Fig. 3A) (2).

Flexibility and conformational heterogeneity of a loop connecting the acceptor binding domain and the C-terminal extension (residues 253–262, linking β8 and α9 in *MtGpgS*; the numbering system for *MtGpgS* is used for both *MaGpgS* and *MtGpgS* throughout this paper, unless stated otherwise) appears to be critical during substrate binding and catalysis in GpgS enzymes (Fig. 3, A and B). In the apo-form of *MtGpgS*, we observed that this flexible loop adopts a double conformation in both monomers of the protein dimer (r.m.s.d. value of 1.88 for six residues; Fig. 3, C and D), a property that was not seen in the previous reported apo crystal structures of GpgS. These conformations correspond to a catalytically active (L<sub>A</sub>, relative occupancy of 60%) and inactive (L<sub>I</sub>, relative occupancy of 40%) states of the loop in the active site. L<sub>A</sub> and L<sub>I</sub> most likely represent distinct energy states of the L loop rather than crystallization artifacts because they do not participate in crystal packing interactions. A detailed analysis of intermolecular interactions showed four residues, Arg<sup>256</sup>, Ala<sup>257</sup>, His<sup>258</sup>, and Arg<sup>261</sup> in the L loop, to be of particular importance. In the inactive L<sub>I</sub> conformation, the Arg<sup>256</sup> makes hydrogen bonds with the side chain OH of Asp<sup>136</sup>, which is part of the Asp-Xaa-Asp motif, and

Glu<sup>212</sup>. In addition, Arg<sup>261</sup> is hydrogen bonded with the lateral chain of Tyr<sup>229</sup>. Although in the active L<sub>A</sub> conformation the two arginine residues conserved the described binding motif, a new hydrogen bond was formed between the main chains of Ala<sup>257</sup> and Ile<sup>138</sup>. Importantly, also found within this loop was His<sup>258</sup>, which plays a fundamental role in metal coordination in GpgS and other GT-A enzymes, including the UDP-GalNAc:polypeptide α-N-acetylgalactosaminyltransferase T1 (GT27 family) and the mannosylglycerate synthase (GT78 family) (41, 51, 52). The side chain of His<sup>258</sup> in the L<sub>A</sub> conformation is in an optimal position to readily coordinate with metal ions, although it is far away from the nucleotide-binding site in the L<sub>I</sub> conformation making van der Waals interaction with the side chain of Tyr<sup>165</sup>.

Notably, the active L<sub>A</sub> conformation of the L loop observed in the apo-form of *MtGpgS* is conserved in two other relevant structural states of the enzyme, the metal·nucleotide or metal·nucleotide sugar donor-bound complexes (Mg<sup>2+</sup>·UDP, Mn<sup>2+</sup>·UDP, and Mn<sup>2+</sup>·UDP-Glc), and the metal·nucleotide acceptor-bound complex (Mn<sup>2+</sup>·UDP-PGA) (Tables 2 and 3 for r.m.s.d. and φ/ψ/ω torsion angle values respectively; Fig. 3D). In all protein·substrate complexes, Arg<sup>256</sup> and Arg<sup>261</sup> slightly change their side chain traces to allow for metal ion coordination and substrate binding. The side chain of Arg<sup>256</sup> participates in Mg<sup>2+</sup> or Mn<sup>2+</sup> coordination and makes hydrogen bonding with Glu<sup>212</sup>, whereas Arg<sup>261</sup> makes electrostatic interaction with the α-phosphate of UDP-Glc. Importantly, the orientation of the key His<sup>258</sup> residue found in the L<sub>A</sub> conformation is preserved in the complexes and coordinates Mg<sup>2+</sup> or Mn<sup>2+</sup> ions. In addition, the hydrogen bonding between Ala<sup>257</sup> and Ile<sup>138</sup> is also conserved. Altogether, the structural data indicated that the conformation of the L loop detected during catalysis is already present in the free enzyme, suggesting that the protein conformation necessary for catalysis is an intrinsic property of GpgS.

**Donor Recognition Site, Two Conformations for the β-Phosphate**—The uridine moiety binds to a pocket in the N-terminal domain mainly defined by the connecting loops β2-α2 (residues 80–87), β3-α3 (residues 50–56), β5-α6 (residues 133–143), α8-α9 (residues 221–230), and L<sub>A</sub>, where it makes a number of hydrophobic and hydrophilic contacts with the protein. Of particular relevance, Ser<sup>81</sup> makes hydrogen bond with the uridyl O<sub>2</sub> providing the basis for the nucleoside specificity. Moreover, the side chain of Tyr<sup>229</sup> makes an important hydrogen bond with the O<sub>5</sub> of the α-phosphate of UDP. Its side chain conformation is also conserved in the apo-form and other ligand-bound forms of the enzyme. Interestingly, the β-phosphate of UDP binds to the enzyme into two different conformations (Fig. 4A). In the first conformation, the β-phosphate is oriented toward the α-face of the ribose ring and in close proximity to the catalytic center. Consequently, the sugar moiety is favorably positioned for its transfer to the acceptor substrate PGA. This conformation has been observed in *MaGpgS*·Mn<sup>2+</sup>·UDP, *MaGpgS*·Mn<sup>2+</sup>·UDP-Glc, *MtGpgS*·Mg<sup>2+</sup>·UDP-PGA, and other GT-A homologous enzymes, including MgS from *Rhodothermus marinus*, which catalyzes the synthesis of α-mannosyl-D-glycerate using GDP-Man as donor sugar (Fig. 4B; family 78) (29, 41, 47, 52). In contrast, we found that in the second conformation, the β-phosphate, is on the contrary oriented toward the β-face of the ribose ring, solvent-exposed, and away from the catalytic

**TABLE 1**
**Data collection, phasing, and refinement statistics**

Values in parentheses are for highest resolution shell.

	<i>MtGpgS</i> apo-form	<i>MtGpgS</i> UDP	<i>MtGpgS</i> ·UDP·PGA·Mn <sup>2+</sup>
<b>Data collection</b>			
Space group	<i>I</i> 4 <sub>1</sub>	<i>I</i> 4 <sub>1</sub>	<i>I</i> 4 <sub>1</sub>
Cell dimensions			
<i>a</i> , <i>b</i> , <i>c</i>	98.85, 98.85, 127.64 Å	98.85, 98.85, 127.64 Å	100.32, 100.32, 127.03 Å
$\alpha$ , $\beta$ , $\gamma$	90, 90, 90°	90, 90, 90°	90, 90, 90°
Resolution	34.95 to 2.60 Å (2.69 to 2.60 Å)	39.08 to 2.99 Å (3.11 to 2.99 Å)	39.36 to 1.98 Å (2.10 to 1.98 Å)
<i>R</i> <sub>sym</sub> or <i>R</i> <sub>merge</sub>	0.106 (0.480)	0.107 (0.413)	0.062 (0.576)
<i>I</i> / $\sigma$ <i>I</i>	8.9 (3.0)	10.3 (3.3)	12.4 (2.0)
Completeness	100% (100%)	100% (100%)	96.9% (98.4%)
Redundancy	7.0 (6.5)	7.2 (7.0)	3.8 (3.8)
<b>Refinement</b>			
Resolution	2.60 Å	2.99 Å	1.98 Å
No. reflections	37,009	12,193	42,399
<i>R</i> <sub>work</sub> / <i>R</i> <sub>free</sub>	0.2147/0.2457	0.2242/0.2447	0.1785/0.2054
No. of atoms			
Protein	2133	2132	2162
Ligand/ion	18	28	53
Water	61	22	221
<i>B</i> -factors			
Protein	61.3	62.3	40.8
Ligand/ion	69.4	72.7	55.4
Water	55.0	46.5	50.3
r.m.s.d.			
Bond lengths	0.016 Å	0.007 Å	0.018 Å
Bond angles	1.429°	0.975°	1.566°

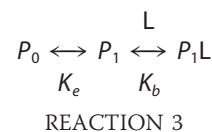
site. Specifically, the  $\beta$ -phosphate rotates 240°, and its O<sub>2</sub> makes a new hydrogen bond with the side chain of Glu<sup>54</sup>. This conformer has been observed in *MtGpgS*·Mn<sup>2+</sup>·UDP·PGA (this study) and in the homologous enzyme MgS from *R. marinus*, and it likely corresponds to the nucleoside diphosphate moiety of UDP-Glc leaving the catalytic site after sugar moiety transfer (52).

**Acceptor Recognition Site**—The acceptor-binding pocket in *MtGpgS* is located on the top of  $\alpha$ -helix 7, which is also involved in protein dimerization. The carboxyl group of PGA makes a hydrogen bond with the side chain of Thr<sup>187</sup>, whereas Arg<sup>185</sup> positions its guanidinium group in close contact with the phosphate moiety (2.88 Å ArgN $\epsilon$  and the PO<sub>4</sub> O<sub>3</sub>; Fig. 4). A conformational change was observed in the connecting loop  $\beta$ 6- $\alpha$ 7, which presents an intrinsic flexibility provided by three consecutive glycine residues. In the *MaGpgS*·Mn<sup>2+</sup>·UDP-Glc complex, which does not contain the acceptor substrate, Gly<sup>183</sup>–Gly<sup>184</sup> occupy the acceptor-binding pocket, whereas in *MtGpgS*·Mn<sup>2+</sup>·UDP·PGA, the equivalent residues are oriented in opposite direction and away from the binding site, allowing for PGA binding. This places the accepting OH<sub>2</sub> group of PGA at ~2.4 Å from the anomeric C1 of the modeled glucose moiety of UDP-Glc. This result is in contrast with a previous report in which the predicted distance between OH<sub>2</sub> atom of PGA and C1 of the glucose moiety was ~5.48 Å, clearly not compatible for the glucose transfer to take place (47). Interestingly, the PGA and D-glycerate groups lie in equivalent positions in *MtGpgS* and MgS glycosyltransferases (MgS·D-glycerate complex; see Ref. 29), where the accepting hydroxyl group is located at ~2.3 Å from the anomeric C1 of the sugar ring. Furthermore, mutation of Thr<sup>139</sup> in MgS (which is equivalent to Thr<sup>187</sup> in *MtGpgS*) resulted in a 1500-fold increase in the *K<sub>m</sub>* for D-glycerate (52), highlighting its role in acceptor binding and suggesting a common acceptor recognition mechanism for GpgS and MgS.

**Thermodynamics of *MtGpgS*-Substrate Interactions**—To investigate further the molecular mechanism of donor and

acceptor substrates binding to *MtGpgS*, binding reactions were studied in solution by isothermal titration calorimetry. First, binding of the donor substrate was studied in the presence of manganese ions. It is worth noting that in the absence of metal ions binding isotherms showed weak affinity confirming the requirement of divalent cations for UDP-Glc binding (data not shown) as observed previously with bovine  $\alpha$ -1,3-galactosyltransferase and more recently with MgS (20, 52). UDP-Glc bound to *MtGpgS* with an apparent stoichiometry of one ligand molecule per protein monomer (Fig. 5). However, the binding isotherm was atypical revealing two clearly detectable reactions, one with decreasing heats of reaction at low ligand to protein molar ratios the other with increasing binding heats at high molar ratios, revealing a complex binding process (Fig. 5A). This binding isotherm could not be fitted to a bimolecular association model.

This peculiar binding process was even better observed with UDP as the heat contribution of the reaction at low UDP to protein molar ratios was greater than with UDP-Glc binding (Fig. 5A). The observation that *MtGpgS* bound both UDP-Glc and UDP with a similar binding process and overall stoichiometries of one nucleotide per protein monomer together with the observation that the heat of the low molar ratio reaction decreased with increasing temperatures from 15 to 35 °C (supplemental Fig. S1) brought us to consider *MtGpgS* protein as being in equilibrium between two conformations, *P*<sub>0</sub> and *P*<sub>1</sub>, with only one conformation, *P*<sub>1</sub>, binding the nucleotide diphosphate ligand (“Experimental Procedure” and Table 4) as shown in Reaction 3,



Within this model, nucleotide diphosphate (L) binding to *P*<sub>1</sub> conformation shifts the *P*<sub>0</sub> *P*<sub>1</sub> conformational equilibrium of

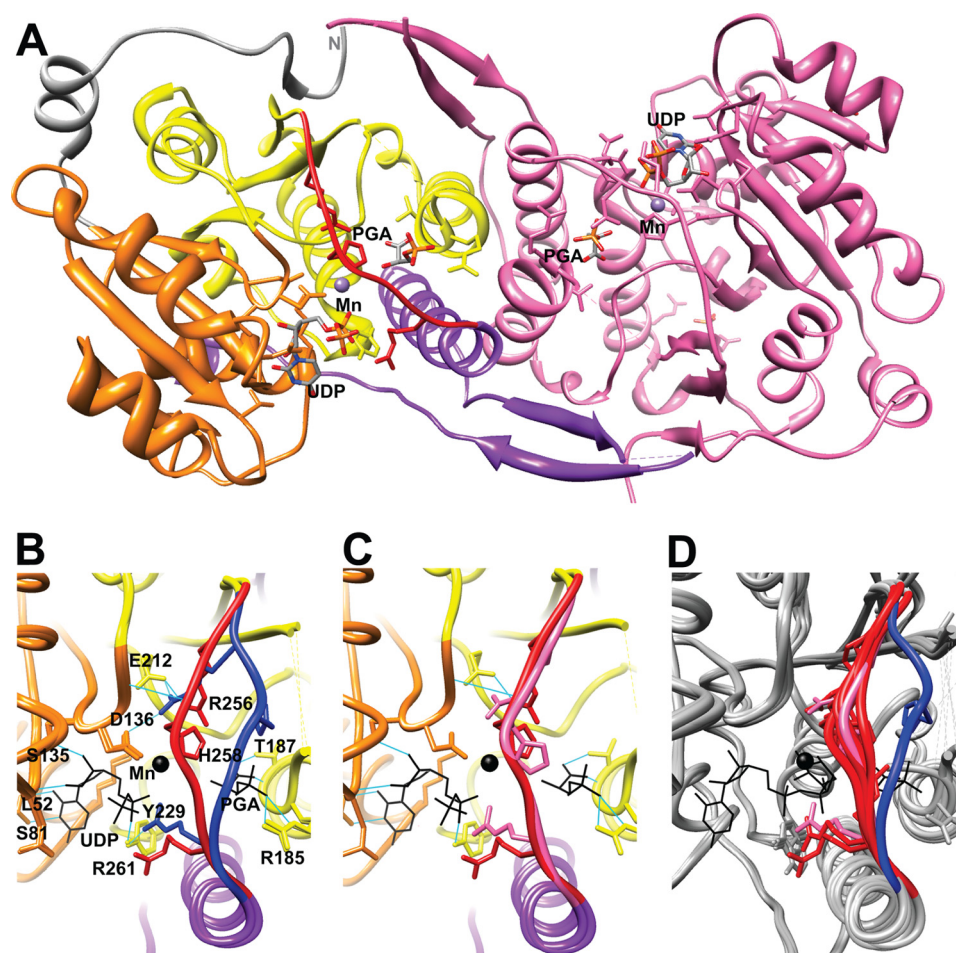


FIGURE 3. **Two different conformations,  $L_A$  and  $L_I$ , for the catalytic loop.** *A*, overall structure of *MtGpgS* in complex with  $Mn^{2+}$ -UDP-PGA. The core of the protein consists of an eight-stranded continuous  $\beta$ -sheet with topology  $\beta_4$ - $\beta_3$ - $\beta_2$ - $\beta_5$ - $\beta_7$ - $\beta_8$ - $\beta_1$  ( $\beta_7$  is antiparallel) flanked by three  $\alpha$ -helices on either side. The sugar donor-binding domain includes residues 45–138 (orange), whereas the acceptor-binding domain is made of residues 139–262 (yellow). A large C-terminal extension (residues 262–323) containing an  $\alpha$ -helix and a two-stranded antiparallel twisted  $\beta$ -sheet ( $\beta_{11}$ - $\beta_{12}$ ), are rich in aromatic residues and involved in protein dimerization (purple). The second monomer is shown in pink. *B*, structural comparison of the catalytic loop as observed in the ternary *MtGpgS*- $Mn^{2+}$ -UDP-PGA (red) complex and in its inactive conformation  $L_I$  in the apo-form (blue). *C*, structural comparison of the catalytic loop as observed in the ternary *MtGpgS*- $Mn^{2+}$ -UDP-PGA (red) complex and in its active conformation  $L_A$  in the apo-form (pink). *D*, structural comparison of selected region of mycobacterial GpgSs. The catalytic loop as observed in binary and ternary complexes of *MaGpgS* and *MtGpgS* are shown in red. The active conformation  $L_A$  in the apo-form is shown in pink. The inactive conformation  $L_I$  in the apo-form of *MtGpgS* is shown in blue.

**TABLE 2**

Root mean square deviation values for the catalytic loop in active and inactive conformations

	<i>MaGpgS</i> $Mn^{2+}$ , UDP, pH 7.0	<i>MtGpgS</i> $Mg^{2+}$ , UDP, pH 5.5	<i>MaGpgS</i> $Mn^{2+}$ , UDP-Glc, pH 7.0	<i>MaGpgS</i> , UDP-Glc, pH 5.5	<i>MtGpgS</i> $Mn^{2+}$ , UDP-PGA
<i>MtGpgS</i> APO $L_A$	0.519	0.549	0.583	0.494	0.566
<i>MtGpgS</i> APO $L_I$	1.901	1.940	2.071	2.071	2.295

the protein toward the bound  $P_1$  conformation. This model allowed precise predictions of the observed binding isotherms (Fig. 5 and supplemental Fig. S1). UDP-Glc bound *MtGpgS* with high affinity and a largely exothermic and enthalpy-driven reaction with a large heat capacity change on binding ( $K_d = 4 \mu M$ ,  $\Delta H/\Delta G = 172\%$ ,  $\Delta C_p = -368 \text{ cal} \cdot (\text{mol} \cdot \text{K})^{-1}$ ; Fig. 5A and Table 4), a set of binding parameters in agreement with the *MaGpgS*/ $Mn^{2+}$ -UDP-Glc crystal structure and the involvement of hydrophilic interactions in sugar donor association (41). With respect to UDP-Glc binding, UDP bound to *MtGpgS* with a 4-fold lower affinity, a 4 kcal/mol smaller enthalpy, and a  $45 \text{ cal} \cdot (\text{mol} \cdot \text{K})^{-1}$  binding heat capacity reduction, revealing the contribution of the glucose moiety to the binding process

(Table 4). Based on best fits of UDP binding isotherms at various temperatures, the apparent amounts of  $P_0$  and free  $P_1$  protein conformations varied from 31 and 69% at 15 °C to 10 and 90% at 35 °C, respectively. At 15 °C, the  $P_0$   $P_1$  transition was largely endothermic ( $\Delta H_e = 7.1 \text{ kcal/mol}$ ) and entropy-driven (supplemental Fig. S1 and Table 4).

The nucleotide binding process was further investigated by testing UMP and uridine binding. Both UMP and uridine bound to *MtGpgS*, however, with one main difference, *i.e.* binding isotherms exhibited one binding transition only that could be precisely fitted to a simple bimolecular association model with a binding stoichiometry of one ligand per protein monomer. Binding was enthalpy-driven with binding parameters

# Conformational Dynamics in GT-A Glycosyltransferases

**TABLE 3**  
 $\phi/\psi/\omega$  torsion angles of the L loop in active conformation

L loop <sup>a</sup>	<i>MtGpgS</i> APO L <sub>A</sub>	<i>MaGpgS</i> APO	<i>MaGpgS</i> Mn <sup>2+</sup> , UDP, pH 7.0	<i>MtGpgS</i> Mg <sup>2+</sup> , UDP, pH 5.5	<i>MaGpgS</i> Mn <sup>2+</sup> , UDP-Glc, pH 7.0	<i>MaGpgS</i> , UDP-Glc, pH 5.5	<i>MtGpgS</i> Mn <sup>2+</sup> , UDP-PGA
Val <sup>255</sup>	-136.6	-81.3	-84.9	-157.2	-116.4	-110.5	-125.5
	144.9	129.2	127.3	122.6	126.5	121.9	143.5
	-175.8	-177.7	178.4	-174.1	177.1	177.5	175.6
Arg <sup>256</sup>	-112.0	-129.2	-117.5	-110.6	-122.6	-112.7	-135.0
	126.5	111.0	105.7	141.9	148.5	130.8	144.0
	170.6	173.5	173.4	177.1	177.5	175.5	177.7
Ala <sup>257</sup>	-111.8	-95.8	-87.6	-121.6	-155.5	-126.2	-124.0
	138.8	150.8	132.1	150.0	134.6	130.7	145.3
	-171.9	178.6	168.2	172.8	176.8	178.7	173.5
His <sup>258</sup>	-158.5	-155.4	-152.3	-167.6	-147.7	-140.4	-162.1
	154.4	175.0	156.2	179.0	-154.5	165.3	177.4
	175.1	179.6	178.2	-176.6	-176.9	174.7	174.0
Arg <sup>259</sup>	-64.4	-81.5	-57.7	-72.1	-72.8	-52.5	-57.6
	89.1	149.0	132.9	103.2	132.2	127.1	136.8
	177.6	-179.8	-178.3	178.1	179.4	179.8	166.3
Asn <sup>260</sup>	-56.7	-67.4	-66.6	-72.5	-80.1	-66.5	-95.1
	166.9	123.1	141.3	138.0	98.9	126.2	109.0
	-143.9	170.9	174.3	-171.9	-177.6	177.5	-179.6
Arg <sup>261</sup>	-141.0	-70.2	-67.9	-104.0	-77.7	-74.7	-68.3
	149.9	134.6	131.1	-174.2	131.4	133.7	154.9
	-178.4	-172.7	172.9	-172.6	176.7	180.0	176.4
Pro <sup>262</sup>	-69.8	-64.2	-61.9	-83.7	-65.2	-63.7	-67.4
	148.0	143.3	136.3	146.5	156.3	139.2	155.6
	-170.2	-171.5	-171.8	180.0	-176.9	-172.3	-173.4

<sup>a</sup> The L loop in *MtGpgS* apo-form and Mg<sup>2+</sup>/UDP/PGA form (Protein Data Bank codes 3E26 and 3E25 (45)) was found in an inactive conformation or partially unmodeled, respectively.

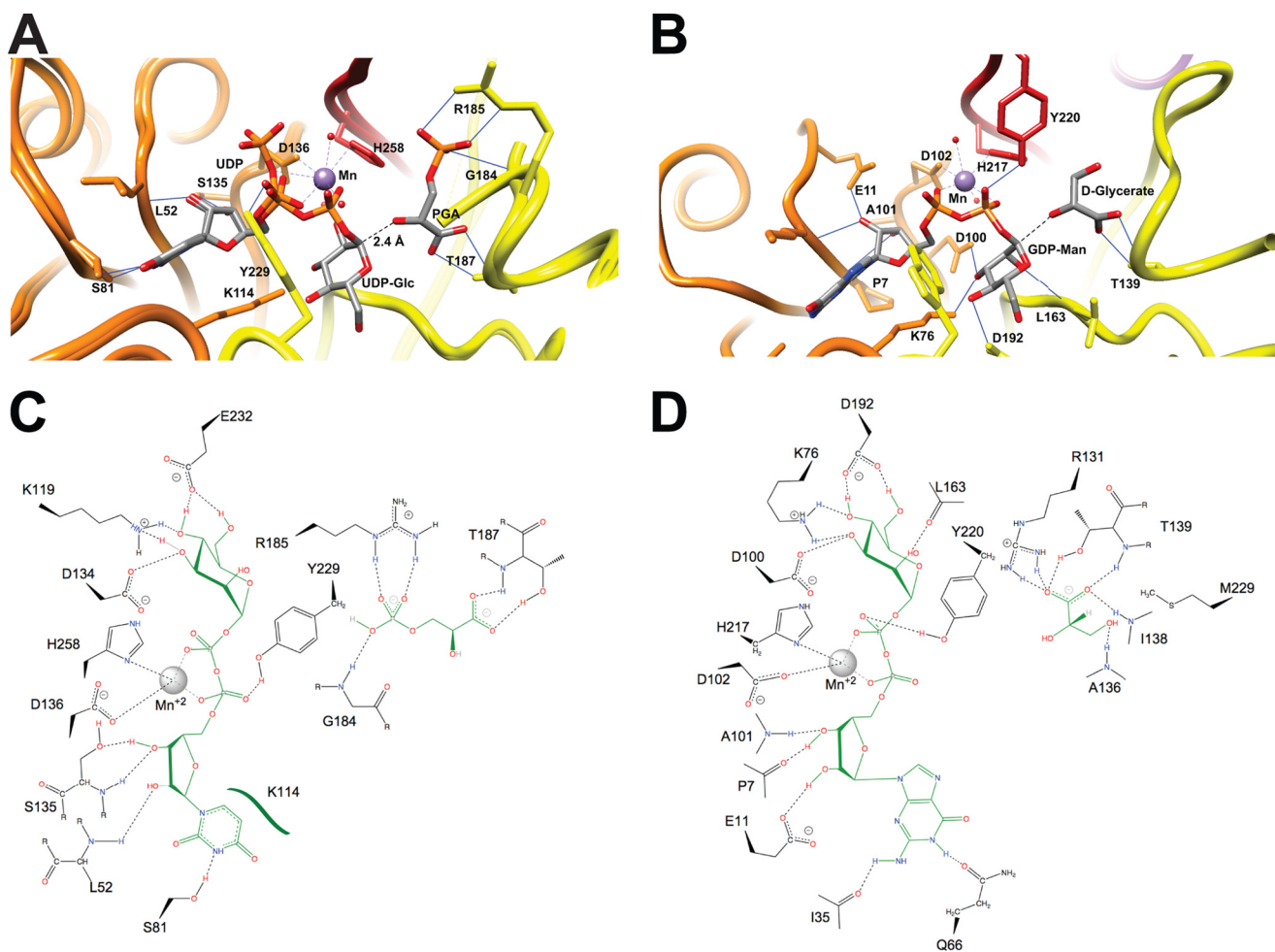


**FIGURE 4. Donor recognition site, two conformations for the  $\alpha$ - and  $\beta$ -phosphates.** *A*, structural comparison of a selected region of the binary *MaGpgS*-Mn<sup>2+</sup>-UDP-Glc (41) and ternary *MtGpgS*-Mn<sup>2+</sup>-UDP-PGA (this study) complexes. The catalytic loop is shown in red. *B*, active site of MgS from *R. marinus* in the same orientation as GpgS. *C* and *D*, schematic representation showing *MtGpgS* and MgS, respectively, associated to their sugar donor and acceptor substrates.

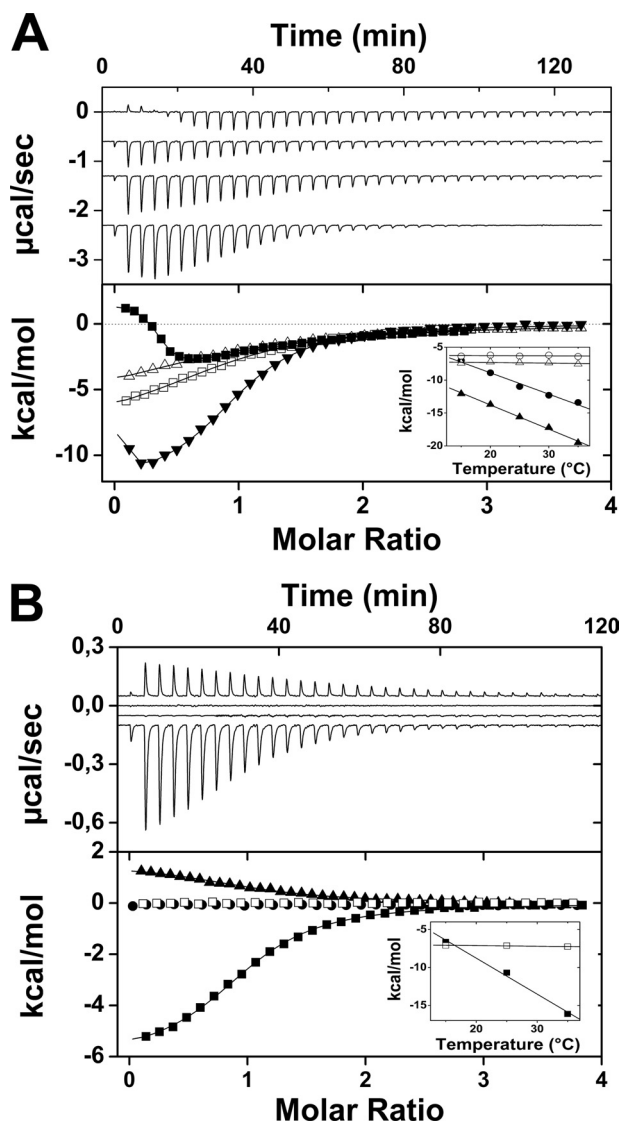


**FIGURE 5. ITC measurements of GpgS-ligand interactions.** A, binding isotherms for the binding of UDP-Glc (▼), UDP (■), UMP (□), and uridine (URI, △) to *MtGpgS* protein at 15 °C. The upper panel shows the raw heat signal for successive injections of a ligand solution into the protein solution. The lower panel shows the integrated heats of injections corrected for the heat of dilution and normalized to ligand concentration. Solid lines correspond to a best fit of the isotherm to the GpgS  $P_0 \leftrightarrow P_1$  conformational equilibrium model for UDP-Glc and UDP (cf. text) and to a bimolecular binding model for URI and UMP. Inset, enthalpies and free energies of binding of UDP (●, ○) and UDP-Glc (▲, △) to the  $P_1$  conformation as a function of temperature. Solid lines correspond to linear fits of the data. B, binding isotherms for the binding of PGA to free *MtGpgS* (●) and to *MtGpgS* complexes formed with UDP (■), UMP (▲), and URI (□) at 15 °C. Inset, same as the inset in A for the binding of PGA to the UDP complex (■, □). B, *MtGpgS* was first titrated with a nucleotide as described in A, and the protein-nucleotide complex formed was then titrated with PGA. Thermodynamic data are reported in Table 4.

similar to those with UDP binding (UDP and uridine binding affinities were 4- and 6-fold lower than UDP-Glc binding affinity, respectively; Fig. 5A and Table 4). An observation clearly indicated that UMP and uridine bound to the two *MtGpgS*  $P_0$  and  $P_1$  protein conformations with equal affinities, respectively. Taken together, these results emphasize the important role of the  $\beta$ - $PO_4$  in stabilizing the donor substrate or product *MtGpgS* complexes in the  $P_1$  conformation, in agreement with the crystal data.

**TABLE 4**

**Thermodynamic parameters of GpgS-ligand interactions at 15°C<sup>a</sup>**

Heat capacity changes ( $\Delta C_p$  on binding of UDP-Glc and UDP to GpgS and on binding of PGA to the GpgS-UDP complex are  $-368 \pm 13 \text{ cal} \cdot (\text{K} \cdot \text{mol})^{-1}$ ,  $-324 \pm 24 \text{ cal} \cdot (\text{K} \cdot \text{mol})^{-1}$ , and  $-475 \pm 53 \text{ cal} \cdot (\text{K} \cdot \text{mol})^{-1}$ , respectively.

Ligand	GpgS	$N$	$K_d$	$\Delta H$	$T\Delta S$	$\Delta H/\Delta G$
				$\mu\text{M}$	$\text{kcal} \cdot \text{mol}^{-1}$	$\text{kcal} \cdot \text{mol}^{-1}$
UDP-Glc	free	$0.8 \pm 0.1$	$4 \pm 1$	$-12.5 \pm 0.1$	$-5.4 \pm 0.2$	172
UDP	free	$0.7 \pm 0.1$	$16 \pm 1$	$-8.4 \pm 0.1$	$-2.1 \pm 0.2$	132
UMP	free	$1.0 \pm 0.1$	$13 \pm 1$	$-8.2 \pm 0.1$	$-1.7 \pm 0.2$	126
uridine	free	$1.0 \pm 0.1$	$21 \pm 1$	$-7.1 \pm 0.1$	$-0.9 \pm 0.2$	114
PGA	free	<i>binding not detected</i>				
PGA	UDP	$1.0 \pm 0.1$	$4 \pm 1$	$-6.1 \pm 0.1$	$1.1 \pm 0.2$	85
PGA	Bound UMP	$1.0 \pm 0.1$	$9 \pm 1$	$1.6 \pm 0.1$	$8.2 \pm 0.2$	-23
PGA	uridine Bound	<i>binding not detected</i>				

Transition <sup>b</sup>	GpgS	amounts		$K_c$	$\Delta H_c$	$T\Delta S_c$	$\Delta H_c / -T\Delta S_c$
		P0	P1				
		%			$\text{kcal} \cdot \text{mol}^{-1}$	$\text{kcal} \cdot \text{mol}^{-1}$	%
$P_0 \leftrightarrow P_1$ free		31	69	$2.2 \pm 0.2$	$7.1 \pm 0.1$	$7.5 \pm 0.2$	-95

<sup>a</sup> Binding parameters resulted from a best fit of the binding isotherms to the GpgS two conformational equilibrium model (see under "Experimental Procedures").

<sup>b</sup> Transition parameters are estimated based on UDP binding to free GpgS.

Second, binding of the acceptor substrate was studied by ITC. PGA bound to the UDP *MtGpgS* complex with a 1:1 stoichiometry with respect to protein monomer, a high affinity with an exothermic and enthalpy-driven reaction ( $K_d = 4 \mu\text{M}$ ,  $\Delta H/\Delta G = 85\%$ ) with a large heat capacity change on binding ( $\Delta C_p = -475 \text{ kcal/mol}$ ) (Fig. 5B and Table 4). PGA also bound to the UMP *MtGpgS* complex with a 1:1 stoichiometry, however, with a completely different binding process. Binding was endothermic and largely entropy-driven with a 2-fold lower binding affinity ( $K_d = 9 \mu\text{M}$ ,  $\Delta H/\Delta G = -23\%$ ; Fig. 1B and Table 1). Although tested at different temperatures, in the presence or absence of metal cations, PGA binding to the uridine *MtGpgS* complex or to free *MtGpgS* could not be detected (Fig. 5B).

Results of the ITC study clearly demonstrated that binding of the donor and acceptor substrates was sequential. Furthermore, UDP and UMP binding to *MtGpgS* leads to the formation of different PGA protein complexes. Altogether, the results of the ITC and x-ray studies make it tempting to hypothesize that  $P_0$  and  $P_1$  *MtGpgS* protein conformations could correspond to the catalytically inactive ( $L_I$ ) and active ( $L_A$ ) states of the protein, respectively, as observed in the protein crystals.

**Overall Conformational Flexibility of *MtGpgS***—To further characterize the effect of substrate binding on the conformation of *MtGpgS*, we performed limited proteolysis experiments. When incubated with trypsin, the enzyme was rapidly degraded (Fig. 6A). Similar profiles to that observed with the unliganded enzyme were obtained when UDP-Glc, UDP, UMP, URI, or PGA alone were present in the reaction mixture. As shown in Fig. 6A, the presence of both UDP and PGA substrates slightly

## Conformational Dynamics in GT-A Glycosyltransferases

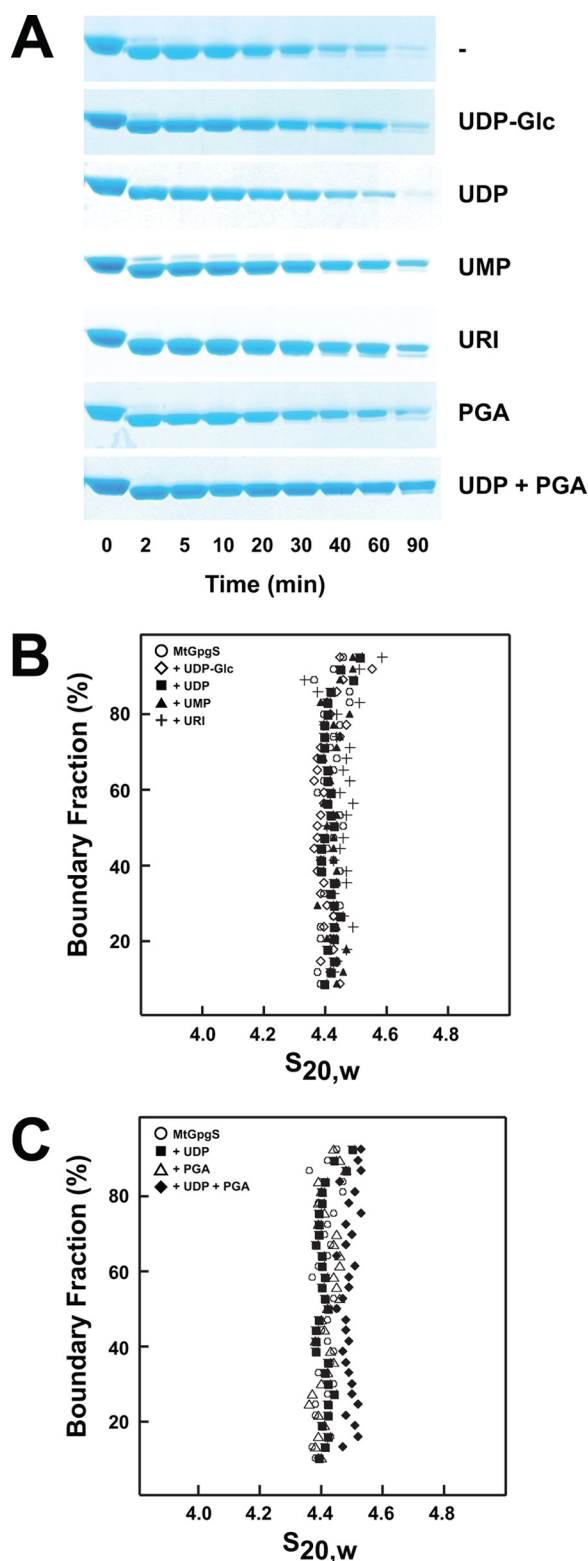


**FIGURE 6. Overall conformational changes in *MtGpgS*.** *A*, trypsin cleavage of *MtGpgS* preincubated with different ligands. *B* and *C*, AUC studies of *MtGpgS* and of *MtGpgS*-ligand complexes. *MtGpgS* (○) was incubated alone or with equimolar amounts of UDP-Glc (◇), UDP (■), UMP (▲), URI (+), PGA (△), and UDP-PGA (◆) prior to sedimentation velocity experiments. The resulting integral distribution of *S* (corrected for water at 20 °C ( $s_{20,w}$ )) is shown.

protected *MtGpgS* from degradation by the protease. Sedimentation velocity AUC studies of pure *MtGpgS* were in agreement with the proteolysis experiments (Fig. 6*B*). The nearly vertical

distribution *s* indicates that *MtGpgS* sedimented as a single homogeneous species with an average sedimentation coefficient of 4.42 *s*, which is consistent with a dimeric protein (71,311 Da). Upon addition of equimolar UDP and PGA, the sedimentation coefficients increased slightly to 4.50 *s*, whereas the presence of UDP-Glc or its derivatives did not significantly affect the *s* values of *MtGpgS*. Taking into account the apparent 1:1 stoichiometry of binding and the relatively minor increase in the molecular weight of *MtGpgS* upon ligand binding, this change in the sedimentation coefficient indicates the formation of a slightly less compact structure. Altogether, our results suggest that although the conformation of the catalytic loop L plays a central role during the catalytic cycle, the overall structure of the enzyme remains unchanged.

**Structural Comparison with GT-A GTs**—To date, the three-dimensional crystal structures of GT-A enzymes in all three relevant functional states of their catalytic cycles (*i.e.* the ligand-free form, the binary complex with bound nucleotide (NDP), or nucleotide sugar (NDP-sugar) donor, and the ternary complex with bound nucleotide (NDP) and acceptor substrates/derivatives) have been reported for families GT6, GT7, GT8, GT13, GT14, GT15, GT29, GT43, and GT64 (2, 11). Interestingly, a careful inspection of all available structures revealed examples wherein very few differences are found between the conformations of the apo- and complexed forms suggesting that, similar to GpgS, the catalytic site of some GT-A enzymes might be preformed before donor and acceptor binding. In the ST3Gal-I sialyltransferase (GT29), there are no significant structural changes of the protein main chain in the active site upon Galβ1,3-GalNAc-α-PhNO<sub>2</sub> or CMP/Galβ1,3-GalNAc-α-PhNO<sub>2</sub> binding, consistent with the random order mechanism determined for this enzyme (53, 54). The α1,2-mannosyltransferase Kre2p/Mnt1p from *Saccharomyces cerevisiae* (GT15), involved in both *N*-linked outer chain and *O*-linked oligosaccharide biosynthesis, displays an r.m.s.d. between the ligand-free form and its binary and ternary complexes of 0.17 and 0.19 Å, respectively (55). Only a limited number of side chain conformational changes occur in the enzyme upon binding of the donor and acceptor substrates. The fact that an acceptor substrate-enzyme binary complex could not be obtained in this case suggests that the acceptor-binding site may only be available after binding of the donor substrate, which is consistent with a sequential ordered mechanism determined for other retaining GT-A GTs. Similarly, the overall structure of the apo-form of the UDP-GlcA:galactosylgalactosylxylosylprotein 3-β-glucuronosyltransferase (GT43) is almost similar to the ternary complex with Mn<sup>2+</sup>·UDP-*N*-acetyllactosamine (r.m.s.d. of 0.38 Å) (56). Interestingly, only the side chains of three basic residues (Lys<sup>153</sup>, Arg<sup>165</sup>, and Arg<sup>313</sup>) undergo conformational changes upon UDP binding. In contrast, a large conformational change induced after donor and/or acceptor binding has been observed in several GT-A enzymes, including the UDP-Gal:β-galactoside α-1,3-galactosyltransferase (GT6) (20), the UDP-Gal:β-GlcNAc β-1,4-galactosyltransferase T1 (GT7) (23), glycogenin (GT8) (57), and the α1,4-*N*-acetylhexosaminyltransferase EXTL2 (GT64) (58).

**Concluding Remarks**—As highlighted by the structural and biophysical evidence presented herein, the intrinsic flexibility

of an accurate region of the active site of GpgS plays a central role during the donor and acceptor substrates recognition that seems to be of significant relevance during the glycosyl transfer. The crystal structure of the apo-form of MtGpgS revealed two distinct conformational states of the protein characterized by a highly dynamic nature of the L loop. The conformation of the L loop in the binary  $Mn^{2+}$ ·UDP-Glc and the ternary  $Mn^{2+}$ ·UDP-PGA complexes displays minor structural rearrangements when compared with the  $L_A$  state in the free enzyme. Essentially the very few differences involve the lateral chains of two basic residues, Arg<sup>256</sup> and Arg<sup>261</sup>, suggesting that the conformation necessary for catalysis is an intrinsic property of GpgS. The crystallographic snapshots of GpgS during its reaction cycle and calorimetric data strongly support a prominent influence of the nucleotide  $\alpha$ - and  $\beta$ -phosphates in substrate binding and catalysis. Whereas the  $\alpha$ -phosphate is stabilized by a stacking interaction with the conserved Tyr<sup>229</sup>, the  $\beta$ -phosphate seems to alternate between two conformations, which likely correspond to the pre- and post-sugar transfer states. Intriguingly, GpgS shows uncommon metal ion preferences for a GT-A enzyme with a broad range of metal cations capable of assisting catalysis.

Recent reports show a remarkable role for protein conformational dynamics in substrate recognition and product release and enzyme catalysis (59–64). These conformational dynamics seem to act locally and allosterically to modulate the affinity and selectivity of enzymes, signaling proteins, and receptors (65). The current scenario shows the conformational dynamics of the L loop of GpgS as a major determinant in metal/substrate association and catalysis and opens the debate of whether a “conformational selection rather than an “induced-fit” mechanism might govern substrate recognition. Nevertheless, further studies would be required to confirm this hypothesis and the occurrence of a similar model in other GT-A glycosyltransferases.

*Acknowledgments*—We gratefully acknowledge Dr. Karolin Luger (Dept. of Biochemistry and Molecular Biology, Colorado State University) for providing us with full access to the protein purification and x-ray crystallography facilities. We also thank to Dr. Karen Dobos (Mycobacteria Research Laboratories, Dept. of Microbiology, Immunology, and Pathology, Colorado State University) for providing us with full access to the protein purification facility, and Dr. Steven McBryant (Dept. of Biochemistry and Molecular Biology, Colorado State University) for help with AUC experiments. We thank the Advanced Light Source and European Synchrotron Radiation Facility for granting access to synchrotron radiation facilities and their staff for the on-site assistance. We also thank all members of the Structural Glycobiology Group (Spain) for valuable scientific discussions.

## REFERENCES

- Rini, J., Esko, J., and Varki, A. (2009) in *Essentials of Glycobiology* (Varki, A., Cummings, R., Esko, J., Freeze, H., Stanley, P., Bertozzi, C. R., Hart, G., and Etzler, M. E., eds) 2nd Ed., Cold Spring Harbor Laboratory Press, Cold Spring Harbor, NY
- Lairson, L. L., Henrissat, B., Davies, G. J., and Withers, S. G. (2008) Glycosyltransferases. Structures, functions, and mechanisms. *Annu. Rev. Biochem.* **77**, 521–555
- Persson, K., Ly, H. D., Dieckelmann, M., Wakarchuk, W. W., Withers, S. G., and Strynadka, N. C. (2001) Crystal structure of the retaining galactosyltransferase LgtC from *Neisseria meningitidis* in complex with donor and acceptor sugar analogs. *Nat. Struct. Biol.* **8**, 166–175
- Gibson, R. P., Turkenburg, J. P., Charnock, S. J., Lloyd, R., and Davies, G. J. (2002) Insights into trehalose synthesis provided by the structure of the retaining glycosyltransferase OtsA. *Chem. Biol.* **9**, 1337–1346
- Frantom, P. A., Coward, J. K., and Blanchard, J. S. (2010) UDP-(5F)-GlcNAc acts as a slow binding inhibitor of MshA, a retaining glycosyltransferase. *J. Am. Chem. Soc.* **132**, 6626–6627
- Errey, J. C., Lee, S. S., Gibson, R. P., Martinez Fleites, C., Barry, C. S., Jung, P. M., O'Sullivan, A. C., Davis, B. G., and Davies, G. J. (2010) Mechanistic insight into enzymatic glycosyl transfer with retention of configuration through analysis of glycomimetic inhibitors. *Angew. Chem. Int. Ed. Engl.* **49**, 1234–1237
- Lee, S. S., Hong, S. Y., Errey, J. C., Izumi, A., Davies, G. J., and Davis, B. G. (2011) Mechanistic evidence for a front-side, S<sub>N</sub>i-type reaction in a retaining glycosyltransferase. *Nat. Chem. Biol.* **7**, 631–638
- Ardèvol, A., and Rovira, C. (2011) The molecular mechanism of enzymatic glycosyl transfer with retention of configuration. Evidence for a short lived oxocarbenium-like species. *Angew. Chem. Int. Ed. Engl.* **50**, 10897–10901
- Gómez, H., Polyak, I., Thiel, W., Lluch, J. M., and Masgrau, L. (2012) Retaining glycosyltransferase mechanism studied by QM/MM methods. Lipopolysaccharyl- $\alpha$ -1,4-galactosyltransferase C transfers  $\alpha$ -galactose via an oxocarbenium ion-like transition state. *J. Am. Chem. Soc.* **134**, 4743–4752
- Cantarel, B. L., Coutinho, P. M., Rancurel, C., Bernard, T., Lombard, V., and Henrissat, B. (2009) The Carbohydrate-Active EnZymes database (CAZy). An expert resource for glycogenomics. *Nucleic Acids Res.* **37**, D233–D238
- Coutinho, P. M., Deleury, E., Davies, G. J., and Henrissat, B. (2003) An evolving hierarchical family classification for glycosyltransferases. *J. Mol. Biol.* **328**, 307–317
- Breton, C., Snajdrová, L., Jeanneau, C., Koca, J., and Imberty, A. (2006) Structures and mechanisms of glycosyltransferases. *Glycobiology* **16**, 29R–37R
- Charnock, S. J., and Davies, G. J. (1999) Structure of the nucleotide-diphospho-sugar transferase, SpsA from *Bacillus subtilis*, in native and nucleotide-complexed forms. *Biochemistry* **38**, 6380–6385
- Brew, K., Tumbale, P., and Acharya, K. R. (2010) Family 6 glycosyltransferases in vertebrates and bacteria. Inactivation and horizontal gene transfer may enhance mutualism between vertebrates and bacteria. *J. Biol. Chem.* **285**, 37121–37127
- Qasba, P. K., Ramakrishnan, B., and Boeggeman, E. (2005) Substrate-induced conformational changes in glycosyltransferases. *Trends Biochem. Sci.* **30**, 53–62
- Ly, H. D., Lougheed, B., Wakarchuk, W. W., and Withers, S. G. (2002) Mechanistic studies of a retaining  $\alpha$ -galactosyltransferase from *Neisseria meningitidis*. *Biochemistry* **41**, 5075–5085
- Morrison, J. F., and Ebner, K. E. (1971) Studies on galactosyltransferase. Kinetic investigations with *N*-acetylglucosamine as the galactosyl group acceptor. *J. Biol. Chem.* **246**, 3977–3984
- Nishikawa, Y., Pegg, W., Paulsen, H., and Schachter, H. (1988) Control of glycoprotein synthesis. Purification and characterization of rabbit liver UDP-*N*-acetylglucosamine: $\alpha$ -3-D-mannoside  $\beta$ -1,2-*N*-acetylglucosaminyltransferase I. *J. Biol. Chem.* **263**, 8270–8281
- Boix, E., Swaminathan, G. J., Zhang, Y., Natesh, R., Brew, K., and Acharya, K. R. (2001) Structure of UDP complex of UDP-galactose: $\beta$ -galactoside- $\alpha$ -1,3-galactosyltransferase at 1.53-Å resolution reveals a conformational change in the catalytically important C terminus. *J. Biol. Chem.* **276**, 48608–48614
- Boix, E., Zhang, Y., Swaminathan, G. J., Brew, K., and Acharya, K. R. (2002) Structural basis of ordered binding of donor and acceptor substrates to the retaining glycosyltransferase,  $\alpha$ -1,3-galactosyltransferase. *J. Biol. Chem.* **277**, 28310–28318
- Ramakrishnan, B., and Qasba, P. K. (2001) Crystal structure of lactose synthase reveals a large conformational change in its catalytic component, the  $\beta$ 1,4-galactosyltransferase-I. *J. Mol. Biol.* **310**, 205–218
- Ramakrishnan, B., Balaji, P. V., and Qasba, P. K. (2002) Crystal structure of

- $\beta$ 1,4-galactosyltransferase complex with UDP-Gal reveals an oligosaccharide acceptor-binding site. *J. Mol. Biol.* **318**, 491–502
23. Ramakrishnan, B., Boeggeman, E., Ramasamy, V., and Qasba, P. K. (2004) Structure and catalytic cycle of  $\beta$ -1,4-galactosyltransferase. *Curr. Opin. Struct. Biol.* **14**, 593–600
  24. Guerin, M. E., Kordulakova, J., Schaeffer, F., Svetlikova, Z., Buschiazzo, A., Giganti, D., Gicquel, B., Mikusova, K., Jackson, M., and Alzari, P. M. (2007) Molecular recognition and interfacial catalysis by the essential phosphatidylinositol mannosyltransferase PimA from mycobacteria. *J. Biol. Chem.* **282**, 20705–20714
  25. Guerin, M. E., Schaeffer, F., Chaffotte, A., Gest, P., Giganti, D., Korduláková, J., van der Woerd, M., Jackson, M., and Alzari, P. M. (2009) Substrate-induced conformational changes in the essential peripheral membrane-associated mannosyltransferase PimA from mycobacteria. Implications for catalysis. *J. Biol. Chem.* **284**, 21613–21625
  26. Unligil, U. M., Zhou, S., Yuwaraj, S., Sarkar, M., Schachter, H., and Rini, J. M. (2000) X-ray crystal structure of rabbit *N*-acetylglucosaminyltransferase. Catalytic mechanism and a new protein superfamily. *EMBO J.* **19**, 5269–5280
  27. Pedersen, L. C., Tsuchida, K., Kitagawa, H., Sugahara, K., Darden, T. A., and Negishi, M. (2000) Heparan/chondroitin sulfate biosynthesis. Structure and mechanism of human glucuronyltransferase I. *J. Biol. Chem.* **275**, 34580–34585
  28. Chiu, C. P., Watts, A. G., Lairson, L. L., Gilbert, M., Lim, D., Wakarchuk, W. W., Withers, S. G., and Strynadka, N. C. (2004) Structural analysis of the sialyltransferase CstII from *Campylobacter jejuni* in complex with a substrate analog. *Nat. Struct. Mol. Biol.* **11**, 163–170
  29. Flint, J., Taylor, E., Yang, M., Bolam, D. N., Tailford, L. E., Martinez-Fleites, C., Dodson, E. J., Davis, B. G., Gilbert, H. J., and Davies, G. J. (2005) Structural dissection and high throughput screening of mannosylglycerate synthase. *Nat. Struct. Mol. Biol.* **12**, 608–614
  30. Jamaluddin, H., Tumbale, P., Withers, S. G., Acharya, K. R., and Brew, K. (2007) Conformational changes induced by binding UDP-2F-galactose to  $\alpha$ -1,3 galactosyltransferase. Implications for catalysis. *J. Mol. Biol.* **369**, 1270–1281
  31. Alfaro, J. A., Zheng, R. B., Persson, M., Letts, J. A., Polakowski, R., Bai, Y., Borisova, S. N., Seto, N. O., Lowary, T. L., Palcic, M. M., and Evans, S. V. (2008) ABO(H) blood group A and B glycosyltransferases recognize substrate via specific conformational changes. *J. Biol. Chem.* **283**, 10097–10108
  32. Jackson, M., and Brennan, P. J. (2009) Polymethylated polysaccharides from *Mycobacterium* species revisited. *J. Biol. Chem.* **284**, 1949–1953
  33. Kaur, D., Pham, H., Larrouy-Maumus, G., Rivière, M., Vissa, V., Guerin, M. E., Puzo, G., Brennan, P. J., and Jackson, M. (2009) Initiation of methylglucose lipopolysaccharide biosynthesis in mycobacteria. *PLoS One* **4**, e5447
  34. Keller, J., and Ballou, C. E. (1968) The 6-*O*-methylglucose-containing lipopolysaccharide of *Mycobacterium phlei*. Identification of the lipid components. *J. Biol. Chem.* **243**, 2905–2910
  35. Machida, Y., and Bloch, K. (1973) Complex formation between mycobacterial polysaccharides and fatty acyl-CoA derivatives. *Proc. Natl. Acad. Sci. U.S.A.* **70**, 1146–1148
  36. Hindsgaul, O., and Ballou, C. E. (1984) Affinity purification of mycobacterial polymethyl polysaccharides and a study of polysaccharide-lipid interactions by  $^1\text{H}$  NMR. *Biochemistry* **23**, 577–584
  37. Yabusaki, K. K., and Ballou, C. E. (1979) Effect of polymethylpolysaccharides on the hydrolysis of palmitoyl-coenzyme A by a thioesterase from *Mycobacterium smegmatis*. *J. Biol. Chem.* **254**, 12314–12317
  38. Yabusaki, K. K., and Ballou, C. E. (1978) Interaction of mycobacterial polymethylpolysaccharides with panaric acid and palmitoyl-coenzyme A. Structural specificity and monomeric dissociation constants. *Proc. Natl. Acad. Sci. U.S.A.* **75**, 691–695
  39. Gest, P., Kaur, D., Pham, H. T., van der Woerd, M., Hansen, E., Brennan, P. J., Jackson, M., and Guerin, M. E. (2008) Preliminary crystallographic analysis of GpgS, a key glycosyltransferase involved in methylglucose lipopolysaccharide biosynthesis in *Mycobacterium tuberculosis*. *Acta Crystallogr. Sect. F Struct. Biol. Cryst. Commun.* **64**, 1121–1124
  40. McCoy, A. J., Grosse-Kunstleve, R. W., Adams, P. D., Winn, M. D., Storoni, L. C., and Read, R. J. (2007) Phaser crystallographic software. *J. Appl. Crystallogr.* **40**, 658–674
  41. Fulton Z., McAlister A., Wilce, M. C., Brammananth, R., Zaker-Tabrizi, L., Perugini, M. A., Bottomley, S. P., Coppel, R. L., Crellin, P. K., Rossjohn, J., and Beddoe, T. (2008) Crystal structure of a UDP-glucose-specific glycosyltransferase from a *Mycobacterium* species. *J. Biol. Chem.* **283**, 27881–27890
  42. Emsley, P., Cowtan, K. (2004) Coot. Model-building tools for molecular graphics. *Acta Crystallogr. D Biol. Crystallogr.* **60**, 2126–2132
  43. Adams, P. D., Grosse-Kunstleve, R. W., Hung, L. W., Ioerger, T. R., McCoy, A. J., Moriarty, N. W., Read, R. J., Sacchettini, J. C., Sauter, N. K., and Terwilliger, T. C. (2002) PHENIX. Building new software for automated crystallographic structure determination. *Acta Crystallogr. D Biol. Crystallogr.* **58**, 1948–1954
  44. Schaeffer, F., Matuschek, M., Guglielmi, G., Miras, I., Alzari, P. M., and Béguin, P. (2002) Duplicated dockerin subdomains of *Clostridium thermocellum* endoglucanase CelD bind to a cohesin domain of the scaffolding protein CipA with distinct thermodynamic parameters and a negative cooperativity. *Biochemistry* **41**, 2106–2114
  45. Wiseman, T., Williston, S., Brandts, J. F., and Lin, L. N. (1989) Rapid measurement of binding constants and heats of binding using a new titration calorimeter. *Anal. Biochem.* **179**, 131–137
  46. Demeler, B., and van Holde, K. E. (2004) Sedimentation velocity analysis of highly heterogeneous systems. *Anal. Biochem.* **335**, 279–288
  47. Pereira, P. J., Empadinhas, N., Albuquerque, L., Sá-Moura, B., da Costa, M. S., and Macedo-Ribeiro, S. (2008) *Mycobacterium tuberculosis* glucosyl-3-phosphoglycerate synthase. Structure of a key enzyme in methylglucose lipopolysaccharide biosynthesis. *PLoS ONE* **3**, e3748
  48. Pettersen, E. F., Goddard, T. D., Huang, C. C., Couch, G. S., Greenblatt, D. M., Meng, E. C., and Ferrin, T. E. (2004) UCSF Chimera, a visualization system for exploratory research and analysis. *J. Comput. Chem.* **25**, 1605–1612
  49. Costa, J., Empadinhas, N., and da Costa, M. S. (2007) Glucosylglycerate biosynthesis in the deepest lineage of the bacteria. Characterization of the thermophilic proteins GpgS and GpgP from *Persephonella marina*. *J. Bacteriol.* **189**, 1648–1654
  50. Empadinhas, N., Pereira, P. J., Albuquerque, L., Costa, J., Sá-Moura, B., Marques, A. T., Macedo-Ribeiro, S., and da Costa, M. S. (2011) Functional and structural characterization of a novel mannosyl-3-phosphoglycerate synthase from *Rubrobacter xylanophilus* reveals its dual substrate specificity. *Mol. Microbiol.* **79**, 76–93
  51. Fritz, T. A., Hurley, J. H., Trinh, L. B., Shiloach, J., and Tabak, L. A. (2004) The beginnings of mucin biosynthesis. the crystal structure of UDP-GalNAc:polypeptide  $\alpha$ -*N*-acetylgalactosaminyltransferase-T1. *Proc. Natl. Acad. Sci. U.S.A.* **101**, 15307–15312
  52. Nielsen, M. M., Suits, M. D., Yang, M., Barry, C. S., Martinez-Fleites, C., Tailford, L. E., Flint, J. E., Dumon, C., Davis, B. G., Gilbert, H. J., and Davies, G. J. (2011) Substrate and metal ion promiscuity in mannosylglycerate synthase. *J. Biol. Chem.* **286**, 15155–15164
  53. Rao, F. V., Rich, J. R., Rakić, B., Buddai, S., Schwartz, M. F., Johnson, K., Bowe, C., Wakarchuk, W. W., Defrees, S., Withers, S. G., and Strynadka, N. C. (2009) Structural insight into mammalian sialyltransferases. *Nat. Struct. Mol. Biol.* **16**, 1186–1188
  54. Rearick, J. I., Sadler, J. E., Paulson, J. C., and Hill, R. L. (1979) Enzymatic characterization of  $\beta$ -D-galactoside  $\alpha$ 2 leads to 3 sialyltransferase from porcine submaxillary gland. *J. Biol. Chem.* **254**, 4444–4451
  55. Lobsanov, Y. D., Romero, P. A., Sleno, B., Yu, B., Yip, P., Herscovics, A., and Howell, P. L. (2004) Structure of Kre2p/Mnt1p. A yeast  $\alpha$ 1,2-mannosyltransferase involved in mannoprotein biosynthesis. *J. Biol. Chem.* **279**, 17921–17931
  56. Kakuda, S., Shiba, T., Ishiguro, M., Tagawa, H., Oka, S., Kajihara, Y., Kawasaki, T., Wakatsuki, S., and Kato, R. (2004) Structural basis for acceptor substrate recognition of a human glucuronyltransferase, GlcAT-P, an enzyme critical in the biosynthesis of the carbohydrate epitope HNK-1. *J. Biol. Chem.* **279**, 22693–22703
  57. Chaikuad, A., Froese, D. S., Berridge, G., von Delft, F., Oppermann, U., and Yue, W. W. (2011) Conformational plasticity of glycogenin and its maltosaccharide substrate during glycogen biogenesis. *Proc. Natl. Acad. Sci.*

- U.S.A.* **108**, 21028–21033
58. Pedersen, L. C., Dong, J., Taniguchi, F., Kitagawa, H., Krahn, J. M., Pedersen, L. G., Sugahara, K., and Negishi, M. (2003) Crystal structure of an  $\alpha$ 1,4-*N*-acetylhexosaminyltransferase (EXTL2), a member of the exostosin gene family involved in heparan sulfate biosynthesis. *J. Biol. Chem.* **278**, 14420–14428
  59. Schwartz, S. D., and Schramm, V. L. (2009) Enzymatic transition states and dynamic motion in barrier crossing. *Nat. Chem. Biol.* **5**, 551–558
  60. Tzeng, S. R., and Kalodimos, C. G. (2009) Dynamic activation of an allosteric regulatory protein. *Nature* **462**, 368–372
  61. Boehr, D. D., Nussinov, R., and Wright, P. E. (2009) The role of dynamic conformational ensembles in biomolecular recognition. *Nat. Chem. Biol.* **5**, 789–796
  62. Smock, R. G., and Gierasch, L. M. (2009) Sending signals dynamically. *Science* **324**, 198–203
  63. Masterson, L. R., Cheng, C., Yu, T., Tonelli, M., Kornev, A., Taylor, S. S., and Veglia, G. (2010) Dynamics connect substrate recognition to catalysis in protein kinase A. *Nat. Chem. Biol.* **6**, 821–828
  64. Marlow, M. S., Dogan, J., Frederick, K. K., Valentine, K. G., and Wand, A. J. (2010) The role of conformational entropy in molecular recognition by calmodulin. *Nat. Chem. Biol.* **6**, 352–358
  65. Hammes-Schiffer, S., and Benkovic, S. J. (2006) Relating protein motion to catalysis. *Annu. Rev. Biochem.* **75**, 519–541
  66. Tuffal, G., Albigot, R., Rivière, M., and Puzo, G. (1998) Newly found 2-*N*-acetyl-2,6-dideoxy- $\beta$ -glucopyranose containing methyl glucose polysaccharides in *M. bovis* BCG. Revised structure of the mycobacterial methyl glucose lipopolysaccharides. *Glycobiology* **8**, 675–684
  67. Kamisango, K., Dell, A., and Ballou, C. E. (1987) Biosynthesis of the mycobacterial *O*-methylglucose lipopolysaccharide. Characterization of putative intermediates in the initiation, elongation, and termination reactions. *J. Biol. Chem.* **262**, 4580–4586